*Progress In Electromagnetics Research B, Vol. 72, 17–30, 2017*

# Metamaterial-Based High-Efficiency Wireless Power Transfer System at 13.56 MHz for Low Power Applications

**Junfeng Chen[1], Zhixia Ding[2], Zhaoyang Hu[1], Shengming Wang[1], Yongzhi Cheng[3], Minghai Liu[1, *], Bin Wei[4], and Songcen Wang[4]**

**Abstract**—Magnetically coupled resonant wireless power transfer (WPT) has been employed in many applications, including wireless charging of portable electronic devices, electric vehicles and powering of implanted biomedical devices. However, transmission efficiency decreases sharply due to divergence of magnetic field, especially in under coupled region. Electromagnetic (EM) metamaterial (MM) can manipulate the direction of EM fields due to its abnormal effective permittivity or permeability. In this paper, an ultra-thin and extremely sub-wavelength magnetic MM is designed for a 13.56 MHz WPT system to enhance magnetic field and its power transfer efficiency (PTE). The WPT systems are investigated theoretically, experimentally and by simulation. A relatively high maximum efficiency improvement of 41.7% is obtained, and the range of efficient power transfer can be greatly extended. The proposed MM structure is very compact and ultra-thin in size compared with early publications for some miniaturized applications. In addition, large area, homogeneous magnetic field is obtained and discussed using the proposed MM. Finally, the proposed MM is applied in a more practical WPT system (with a low power light bulb load) to reveal its effects. The bulb brightness intuitively verifies the efficiency improvement in the WPT system with the MM.

## 1. INTRODUCTION

Wireless power transfer (WPT) has attracted much attention from researchers due to its potential applications such as portable electronic devices and electric vehicles. The concept of WPT technology was first proposed by Nikola Tesla more than a century ago [1]. Most existing and commercially available WPT systems are based on inductive coupling [2], in which charging equipment and power source need to be close between each other. So the application of such systems is limited due to this obvious drawback. For energy transfer over a long distance, the approach of microwave power transmission [3], namely a radiant WPT technology, is commonly used. However, the large antenna size, high-power transmission and electromagnetic (EM) unsafety limit its consumer applications. The mid-range non-radiant WPT technology was first reported by Kurs et al. [4]. This technology is based on magnetic resonance theory and relies on near-field resonant coupling. The magnetic resonance is particularly suitable for daily applications because the interactions with environmental objects are reduced even further. So near-field magnetic resonance is more promising as a practical WPT technology. However, the power transfer efficiency (PTE) drops dramatically for distances larger than several coil diameters [5, 6].

*Received 15 July 2016, Accepted 2 December 2016, Scheduled 15 December 2016*

* Corresponding author: Minghai Liu (mhliu@mail.hust.edu.cn).

[1] State Key Laboratory of Advanced Electromagnetic Engineering and Technology, School of Electrical and Electronic Engineering, Huazhong University of Science and Technology, Wuhan 430074, China. [2] School of Automation, Huazhong University of Science and Technology, Wuhan 430074, China. [3] Engineering Research Center for Metallurgical Automation and Detecting Technology Ministry of Education, Wuhan University of Science and Technology, Wuhan 430081, China. [4] China Electric Power Research Institute, Beijing 100192, China.

To further extend the transfer distance and enhance efficiency, additional, passive, relay resonators may be helpful. In [7], Lee et al. proposed a method of relay resonators arranged in domino forms. It is observed that power transmission range and efficiency was extended greatly. The intermediate resonators which receive the magnetic field from the primary coil then transmit the field to the secondary coil. In fact, this method is about resonant coils analysis, that is, a design procedure to maximize efficiency in three-, four-, five-coils inductive links for magnetic field repeaters to maximize their benefits [8]. Recently, the usage of MMs for WPT systems has been reported [9–14]. Some comparisons between the repeater and MMs are proposed for applications in WPT [15]. The analysis presented that the physical mechanisms of the enhanced coupling of the methods were not same, and it was shown that while each achieved enhanced coupling in different ways, both could increase WPT efficiency. MMs can provide versatile and various tunable functions in WPT, which is not achievable using a simple repeater. For example, the MMs are promising in omnidirectional WPT systems [9]. A nonidentical coils WPT system with MM cavity is also reported by Pham et al. [11]. However, the WPT systems with MMs need to be further investigated. As we all know, MMs have shown great power of controlling the EM waves, which is mainly about the propagation property of far field. However, investigations on near field problem are lacking. In 2000, a negative refractive index MM lens was proposed in theory by Pendry [16], which could focus the propagating waves and enhance the near-field evanescent waves, thereby achieving perfect image reconstruction. The property of MMs, i.e., evanescent wave amplification, is of interest to WPT because the resonant coupling is essentially coupling of near-field evanescent waves. Therefore, we can use MMs to work at megahertz (MHz) band WPT systems. Recently, Urzhumov and Smith [17], Choi and Seo [18], Huang et al. [19], Wang et al. [20, 21] and Lipworth et al. [22] successively reported that efficient WPT systems can be achieved using MMs. In 2011, a theoretical analysis was presented by Urzhumov and Smith, which was about the possibility of using MM to enhance the mutual coupling between magnetic dipoles and thereby the efficiency of WPT system based on simplified assumptions [17]. Then Wang et al. [20] showed that MM could be utilized to enhance the evanescent-wave coupling for enhancing power transfer. They were able to increase the PTE from 17% to 35% using 3D MM for a 27.12 MHz system, at a moderate distance of 0.5 m. Experimental investigation of anisotropic MM for high efficiency WPT was designed at around 6.5 MHz by Ranaweera et al. [23, 24]. The measured efficiencies were 71.1% and 54.3% at a 0.6 and 1.0 m distance, respectively. At a 1.0 m distance, their efficiency performance had a 270% improvement with two MM slabs. In addition, it is shown that a significant efficiency enhancement of WPT with MM also can be obtained under coil misalignment. The performance of MM for WPT system has been proved effective in various environments. However, early reported MMs may be too thick and large in size to increase the PTE and efficient transfer distance, which may limit their practical applications. Therefore, a thin and compact MM for WPT working in ISM band is needed.

Motivated by the above discussions, in this paper, we design an ultra-thin and assembled planar MM structure for 13.56 MHz WPT system numerically and experimentally, which consists of a single-sided periodic array of the capacitive loaded spiral resonators (CLSRs) by FR-4 substrate. The main contribution of this paper lies in the following aspects. First, the MM structure is very compact and ultra-thin in size. The unit cell of conventional split-ring resonator (SRR) MM is approximate 1/10 of the resonant wavelength, while the current design is about 1/158. Second, a relatively high maximum efficiency improvement of 41.7% is obtained compared with some early publications. Therefore, the proposed structure is promising to be a good candidate using in WPT system for low power portable electronic devices with the advantages of high efficiency, light-weighted, ultra-thin and fabrication simplicity.

The organization of this paper is as follows. The MM design and analysis of its effective EM properties are introduced in Section 2. Then, theoretical analysis, full-wave simulation and experiments are given to demonstrate both the WPT systems with and without MM in Section 3. Some discussions are summarized in Section 4. Finally, conclusions are drawn in Section 5.

## 2. METAMATERIAL DESIGN

In previous reports, a negative index MM has the properties of negative permeability $\mu$ and negative permittivity $\varepsilon$ simultaneously. However, highly sub-wavelength negative MMs make the magnetic field

and electric field decouple, thus magnetic field and evanescent wave amplification can be achieved by only negative $\mu$ [16, 25]. Negative permeability MMs are commonly realized using planar arrays of SRRs or SRs [25–27]. In most resonant WPT systems, frequencies are commonly encountered in the low-MHz range at HF band, and their sizes are much smaller than working wavelength, which fall in the deep sub-wavelength limit. Magnetically coupled resonant WPT system achieves the effective power transfer based on coupling of evanescent near fields. Therefore, in our work, only a negative effective $\mu$, instead of double negative index MMs, is used for magnetic field and PTE enhancement in magnetically coupled resonant WPT system for simplicity.

Before implementing simulation and experiment with a WPT system, it is necessary to investigate how evanescent field is affected, when the magnetic MM works. It is seen that the evanescent field will be refocused when the magnetic field is incident on the negative effective permeability MM, as shown in Figure 1(a) [28]. To increase the PTE of a resonant WPT systems, it is required to increase the mutual inductive coupling between the Tx and Rx coil resonators [19]. Because the distance between the Tx coil and Rx coil is so much smaller than the wavelength, the relevant field distribution is quasistatic and the inductive coupling relates mainly to the amount of magnetic flux emanating from the primary coil that is captured by the secondary coil. As shown in Figure 1(b), obviously, the magnetic field can be focused and enhanced around the Rx coil by using the negative effective permeability MM. In other words, enhancing coupling efficiency equates to modifying the field distribution, which in turn means focusing or otherwise controlling the near fields.

In our work, we design an ultra-thin (2 mm) and assembled CLSRs magnetic MM with a lossy FR-4

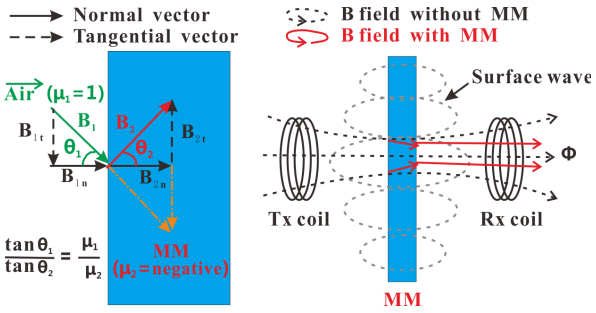


**Figure 1.** (a) Boundary condition of the magnetic field between air and MM. (b) Magnetic field direction with and without MM, in which the Tx and Rx represent transmitter and receiver, respectively.

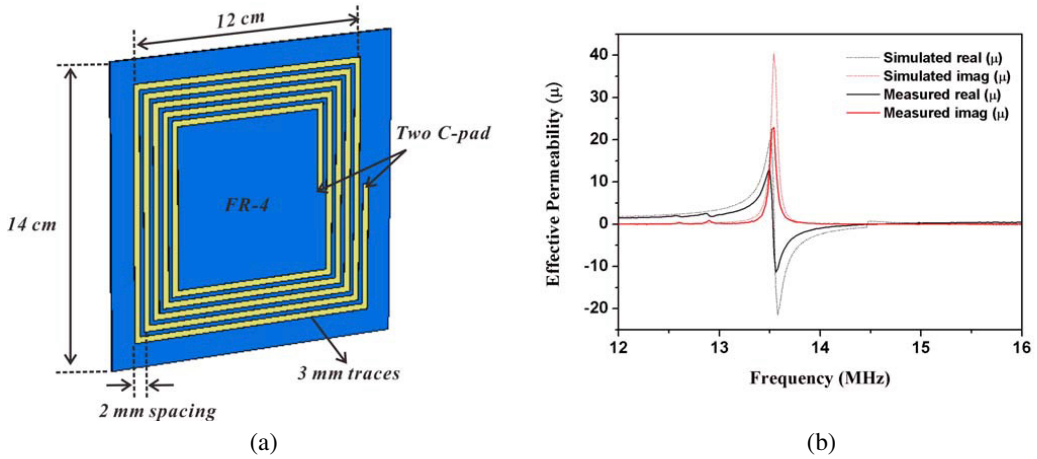


**Figure 2.** (a) Schematic of a unit cell for the used MM. Vias connect the ends of the strip on the front to solder pads for a lumped capacitor (C-pads) on the back. (b) Simulated and measured results of the effective permeability.

substrate to achieve negative effective permeability. The CLSRs structure is designed and optimized by CST Microwave Studio. Figure 2(a) shows the schematic of a unit cell for the CLSRs. Each unit cell consists of a single layer printed circuit board (PCB) planar copper strips with a lumped capacitor of 39 pF that produces its resonant frequency around 13.56 MHz. These extremely sub-wavelength planar magnetic MMs can be characterized by retrieval of optical constants for the structures [25, 29]. For the sake of clarity, results of the retrieved effective permeability [23, 30–33] of the proposed structure are shown in Figure 2(b). It is obvious that the designed MM slab has negative permeability at the resonant frequencies around 13.56 MHz.

## 3. SIMULATION AND EXPERIMENTAL RESULTS OF WPT SYSTEMS

### 3.1. Design and Analysis of Tx and Rx Coils for WPT

To verify the proposed MM effect, we built a symmetric WPT system consisting of four coils as shown in Figure 3. Tx coil and Rx coil structures are square spirals: coil size is 13 × 13 cm, copper wire radius 0.5 mm, a pitch of 10 mm, and 5 turns. Two identical feeding loops consist of a single copper coil, in which the outer diameter and wire radius are 10 cm and 1.25 mm, respectively. A Microtest 6630 Impedance Analyzer (made in Taiwan) is used to measure the coil parameters. The measured coil parameters are shown in Table 1. To tune Tx and Rx coils accurately, flexible coaxial-like capacitors are used to adjust a target resonant frequency and to prevent variation of the target resonant frequency due to external interfering objects. Additionally, this capacitor has property of low loss, which leads to high Q-factor for the entire resonator [34].

Generally, multi-circle spiral coils are used to fabricate resonators for WPT systems. Here, square spiral coils are built for the proposed system because of their simple fabrication. The investigation of system transmission performance should begin with the analytical analysis of the mutual inductance.

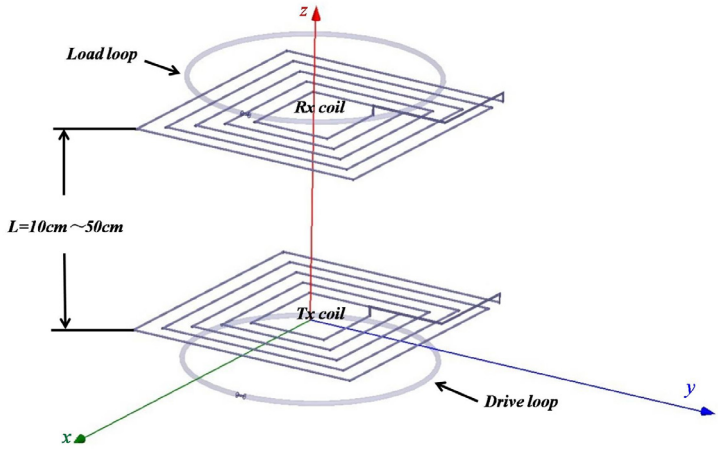


**Figure 3.** Design of the original model of WPT system.

**Table 1.** Measured electrical parameters of coils.

| | Inductance (μH) | Resistance (Ω) | Q (unloaded) 13.56 MHz | Resonant freq. (MHz) |
|---|---|---|---|---|
| Drive loop | 0.27 | 0.61 | 37.8 | — |
| Tx coil | 3.13 | 1.90 | 140.3 | 13.62 |
| Rx coil | 3.12 | 1.87 | 142.1 | 13.48 |
| Load loop | 0.26 | 0.71 | 30.5 | — |

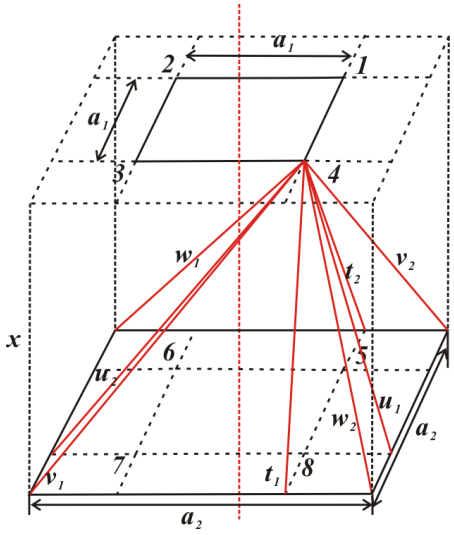


**Figure 4.** Schematic of two nonidentical square coaxial loops, the ends 5, 6, 7, 8 are front projection points of the upper loop.

For the simplest case, both the Tx and Rx of the WPT system are single turn square loop whose side lengths are $a_1$ and $a_2$, respectively, and are placed face-to-face with a distance $x$. The mutual inductance $M$ can be calculated through the function $M(x)$ defined as Eq. (1), where $v_1$, $t_1$, $t_2$, $w_1$, and $w_2$ are shown in Figure 4 [35]. The other corresponding variables are also clearly depicted in Figure 4. Then, the coupling coefficient $k$ can be calculated as Eq. (2), where $L_t$ and $L_r$ are self inductances of the Tx and Rx coils, respectively.

$$M(x) = \frac{\mu_0}{\pi}\left[(a_1+a_2)\ln\left(\frac{a_1+a_2+2v_1}{a_1+a_2+2w_1}\frac{t_2}{t_1}\right)-(a_2-a_1)\ln\left(\frac{a_2-a_1+2w_2}{a_2-a_1+2v_1}\frac{t_2}{t_1}\right)-2(2v_1-w_1-w_2)\right] \quad (1)$$

$$k(x) = \frac{M(x)}{\sqrt{L_t L_r}} \quad (2)$$

According to Eqs. (1) and (2), $M(x)$ between two square spiral coils can be obtained by approximating superposition calculation of concentric square coils, making more convenient to

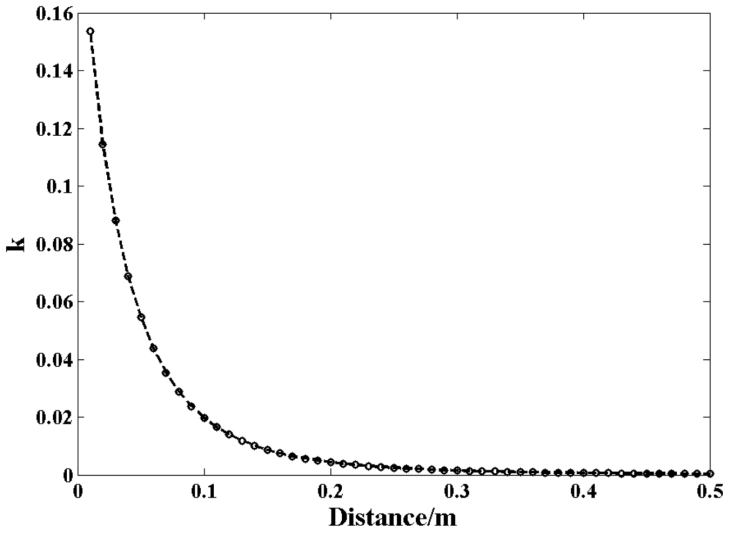


**Figure 5.** Calculation result $k$ of the square spiral coils.

characterize the transfer function of WPT system in theoretical calculation. Additionally, the function of coupling coefficient $k$ versus transfer distance $x$ is also depicted as shown in Figure 5.

### 3.2. Theoretical Calculation of WPT System

Generally, the resonant system can be represented in terms of equivalent lumped circuit elements ($L$, $C$, and $R$). The circuit model of the proposed original WPT system is shown in Figure 6. Four series-resonant circuits linked by mutual inductive coupling are proposed. The resonant WPT system can be seen as a two-port network in which one port is excited by a source and the other outputs fed by a load. In the primary side, $R_s$ is output impedance of the source, $L_1$, $R_1$, $C_1$ are lumped circuit parameters of the one-turn drive loop, and $L_2$, $R_2$, $C_2$ the Tx coil. The geometry of the Tx coil determines its self-capacitance and the coaxial-like capacitor is added to make the drive loop resonant at the target frequency, so $C_2$ is the total resonant capacitor of the Tx coil. Inductors $L_1$ and $L_2$ are connected with coupling coefficient $k_{12}$, and the receive side is defined similarly. It is note that the coupling coefficient between two coils varies with the change of distance between them. Moreover, in the two-port network, impedance matching can be adjusted by the distances between single turn loop and coil resonator.

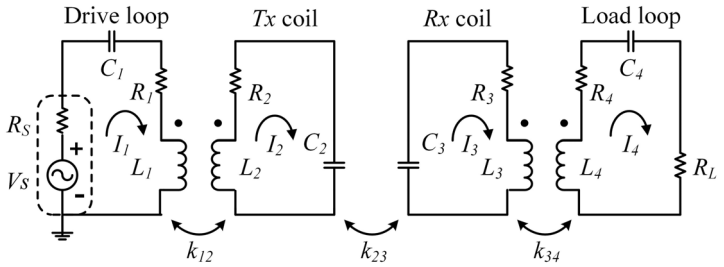


**Figure 6.** Equivalent circuit model of the original WPT system. Each of the four coils is modeled as series resonators, in which the mutual inductances of nonadjacent coils are omitted for simplicity.

Based on the circuit model, the transfer characteristics of the WPT system can be analyzed conveniently [5]. For the sake of simplicity, only the adjacent coils coupling terms are considered in the following analysis. Then, we go back to the equivalent circuit, where Kirchhoff's voltage law (KVL) can be applied to determine the currents in each resonant circuit in Eq. (3), where the coupling coefficient is defined in Eq. (2).

$$\begin{aligned}
&I_1\left(Rs + R_1 + j\omega L_1 + \frac{1}{j\omega C_1}\right) + j\omega I_2 M_{12} = Vs \\
&I_2\left(R_2 + j\omega L_2 + \frac{1}{j\omega C_2}\right) + j\omega(I_1 M_{12} - I_3 M_{23}) = 0 \\
&I_3\left(R_3 + j\omega L_3 + \frac{1}{j\omega C_3}\right) + j\omega(I_4 M_{34} - I_2 M_{23}) = 0 \\
&I_4\left(R_L + R_4 + j\omega L_4 + \frac{1}{j\omega C_4}\right) + j\omega I_3 M_{34} = 0
\end{aligned} \tag{3}$$

$$\frac{V_L}{V_S} = \frac{i\omega^3 k_{12}k_{23}k_{34}L_2L_3\sqrt{L_1L_4}R_L}{\left(k_{12}^2k_{34}^2L_1L_2L_3L_4\omega^4 + Z_1Z_2Z_3Z_4 + \omega^2\left(k_{12}^2L_1L_2Z_3Z_4 + k_{23}^2L_2L_3Z_1Z_4 + k_{34}^2L_3L_4Z_1Z_2\right)\right)} \tag{4}$$

$$\begin{aligned}
Z_1 &= R_1 + R_S + j\omega L_1 - j/(\omega C_1) \\
Z_2 &= R_2 + j\omega L_2 - j/(\omega C_2) \\
Z_3 &= R_3 + j\omega L_3 - j/(\omega C_3) \\
Z_4 &= R_4 + R_L + j\omega L_4 - j/(\omega C_4)
\end{aligned} \tag{5}$$

According to these four KVL equations, the voltage across the load can be solved with the substitution in Eq. (5). The system transfer function in Eq. (4) is obtained. The transfer function

plot is depicted in Figure 7. This plot shows $S_{21}$ magnitude as a function of frequency and coupling coefficient $k_{23}$. By using the scattering parameters, the function of PTE is defined as $\eta = |S_{21}|^2$ when the network is matching at both ports [5, 36]. At the same time, the linear magnitude of the scattering parameter $|S_{21}|$ can be conveniently measured using a vector network analyzer (VNA) in the experiments and for later comparison. As shown in Eq. (6), the equivalent $S_{21}$ parameter is given by [37, 38]

$$S_{21} = 2\frac{V_L}{V_S}\left(\frac{R_S}{R_L}\right)^{1/2} \tag{6}$$

In Figure 7, frequency splitting is clearly visible as the value of transfer distance ($L$) is decreased, namely, $k_{23}$ is increased. It is found that the frequency separation occurs as the coupling between the coils increases and disappears with decreasing of the coupling until the two modes converge at the system resonant frequency ($f_0 = 13.56\,\text{MHz}$). According to [5], this point is called the critical coupling ($k_{\text{critical}}$) point and represents the farthest distance at which maximum PTE is still achievable (since $k_{23}$ is proportional to $1/L^3$), namely, a point at which the WPT system can no longer drive the load at its maximum efficiency. When $k_{23}$ is greater than kcritical, the system is said to be over coupled, and operating at either resonance will result in maximum PTE. Conversely, when $k_{23}$ is less than $k_{\text{critical}}$, the system is under coupled, and the amount of power delivered to the load begins to fall off dramatically with $L$. Obviously, once transfer distance exceeds the critical coupling point, the PTE drops sharply. To address this problem, magnetic MM will work.

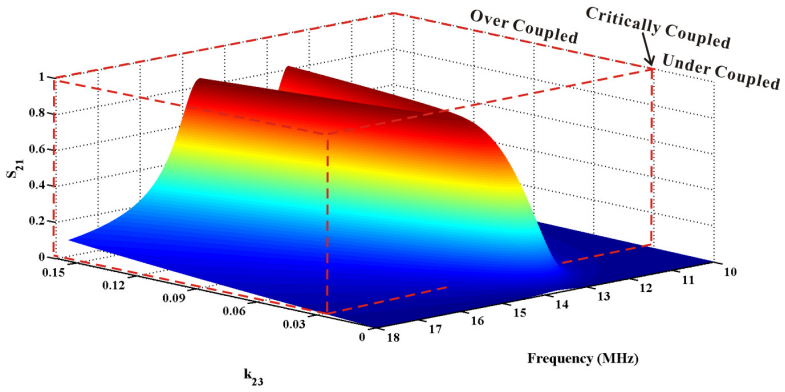


**Figure 7.** $S_{21}$ magnitude as a function of frequency and Tx-to-Rx coupling $k_{23}$ for the proposed circuit model. The highlighted red volume is the over coupled region, where frequency splitting occurs [5].

### 3.3. Simulation and Experimental Results

To further demonstrate the transfer characteristics of the proposed WPT system (without MM) around the critical coupling point, PTEs are investigated by calculation, simulation and experiment. As shown in Figure 8, the obtained results indicate that the proposed WPT system achieved a maximum PTE ($|S_{21}|^2$) [20, 36] of 85.2% at a transfer distance of 13 cm (around the critical coupling point), and the corresponding bandwidth is up to about 1 MHz. The agreement between the theoretical, simulation and the experimental data is excellent. The slight difference between the measured and calculated results may be due to calculation errors, fabrication accuracy and measurement errors. The results shown that a good WPT system was designed before investigations of this system with MM.

To examine near-field evanescent wave coupling by the MM, we firstly performed EM simulations. Figure 9 shows a comparison of the magnetic field magnitude distributions with and without MM at transfer distance of 30 cm, respectively. Compared with the system without MM, the magnetic field intensity between the Tx and Rx coils with MM is considerably increased, as shown in Figure 9(b). It is demonstrated that the magnetic field is focused and enhanced by the negative effective permeability MM slab, which intuitively verifies the validity of the theoretical analysis in Section 2. We also observe strong surface waves existing on both sides of the MM slab, which is responsible for the increased

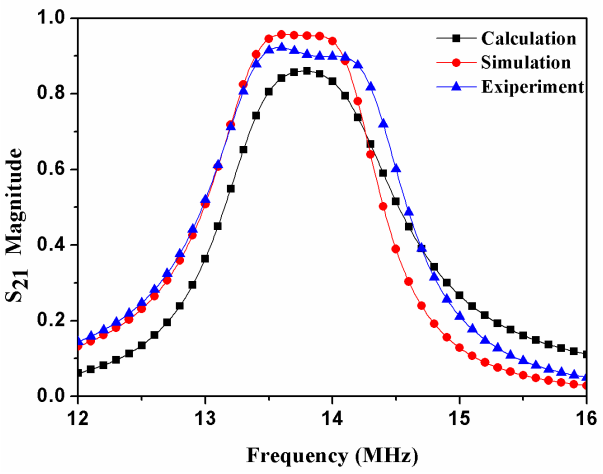


**Figure 8.** Comparison of theoretical, simulation and the experimental results of $S_{21}$ around the critical coupling point.

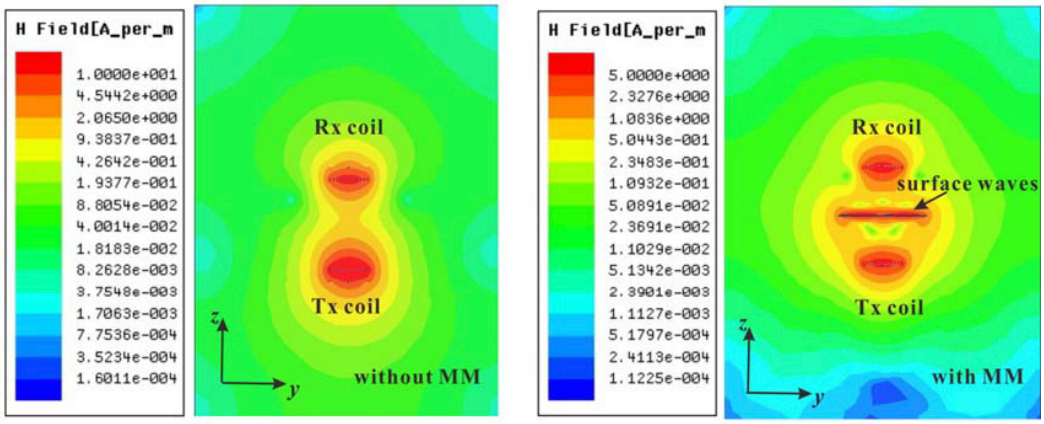


(a) (b)

**Figure 9.** Comparison of magnetic field distribution of WPT system (a) with and (b) without MM, $z$ direction is along with the coil axis as shown in Figure 3.

magnetic coupling [19]. The surface waves are coupled to the decaying evanescent wave from the Tx coil in such a way that the amplitude of the evanescent wave is enhanced [39]. In addition, MMs exhibit a high degree of freedom in assembling, because the bulky effect of them always holds due to their ultra-sub-wavelength property. Good performance in magnetic field homogenization can also be realized when fine four unit patches are assembled squarely to form a $2 \times 2$-unit array, as shown in Figure 10(b). For comparison, the original magnetic field distribution without MM at the same plane is also shown as Figure 10(a). To further enlarge the uniform area, one can simply increase the number of unit cells of MM.

Then, we observe the power transfer of systems with and without MM using the EM simulations. The two cases of WPT systems are simulated by the EM simulator for linear magnitude parameter $|S_{21}|$, which can be conveniently measured using a VNA as mentioned above. The simulation PTEs at different transmission distances were characterized in the cases of both the WPT systems with and without the MM slab. According to the results, the decrease rate of PTE with the increasing of transmission distance of the WPT system using MM is lower than that of the WPT system without MM. In the simulations, the MM slab is located in the middle of the WPT due to its symmetry.

For experiments, a $2 \times 2$ unit cells MM slab is assembled loading in WPT system. Experimental

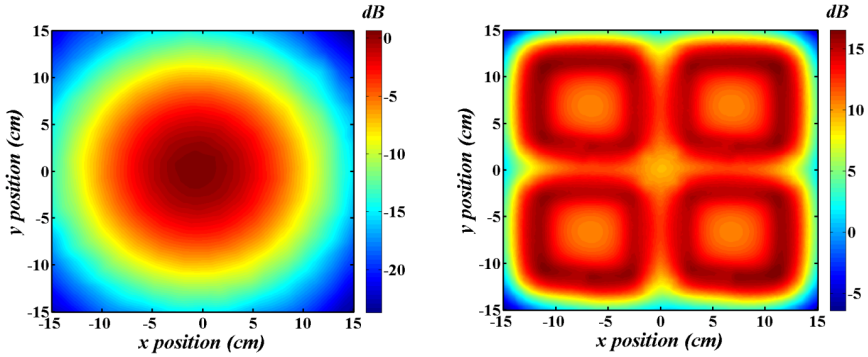


**Figure 10.** Simulation normalized magnetic field distribution of the plane above the Tx by 16 cm (above the MM slab by 1 cm) (a) without MM (b) with MM.

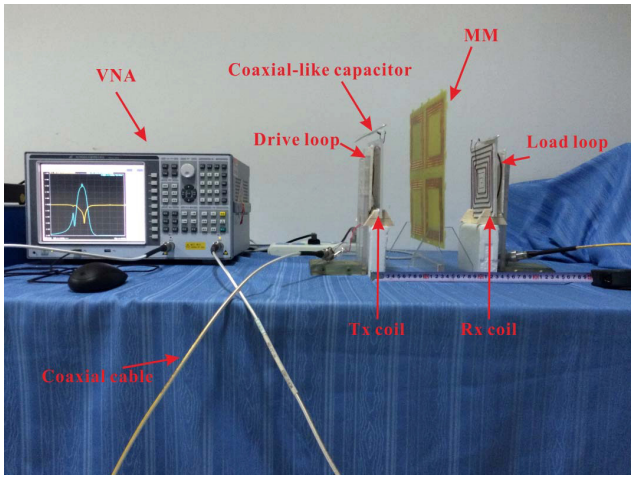


**Figure 11.** Experimental setup of the WPT system with MM slab.

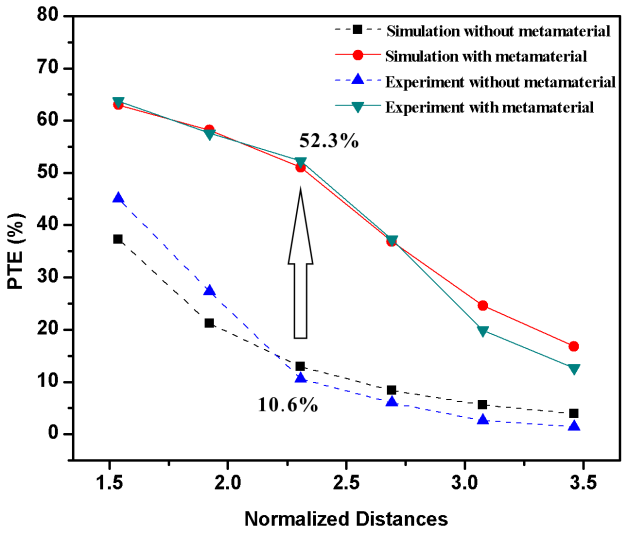


**Figure 12.** PTE versus transmission distance with and without MM.

setup of the resonant system is shown in Figure 11. An AV-3656A VNA (made by NO. 41 Research Institute of China Electronics Technology Group Corp.) was used to measure the $S$-parameters of the WPT system. To verify the enhancement of the WPT system by using CLSRs MM, the four-coil systems integrated with and without MM slab are investigated by the experiments, respectively. The coaxial-like capacitors were used to tune the resonant frequency of WPT system.

According to simulation results, we first placed Tx and Rx coils 30 cm apart, and they were connected to VNA to evaluate transfer power enhancement by MM. For consistency, we characterize the relative power transmission of the WPT system using $|S_{21}|^2$ [20, 36]. The PTEs of WPT systems with and without MM were measured respectively. It can be observed that the transmission and reflection coefficients of a single spiral structure are near the same with the ones of multiple periodic spiral structures (not shown). It also can be expected that the MM property (including permittivity and permeability) of a single spiral structure are near the same with the ones of multiple periodic spiral structures [25, 38]. For the sake of simplicity, we only took the assembled $2 \times 2$ unit cells slab as an example in our study. The impedance mismatch caused by the insertion of MM was removed using a variable coupling method [40]. In order to examine the useful operating range of the WPT systems, the measured PTEs versus the transmission distance were also investigated in the cases of both the

WPT systems with and without MM. Efficiency measurements are taken for transfer distances from 10 to 60 cm, and the results are compared with those in previously published works in Section 4. Due to different coil sizes, the distance on the $x$-axis is normalized to the outer radius of the coil resonators. As shown in Figure 12, the decrease rate of the PTE with the increasing of transmission distance of the WPT system with MM slab is lower than that of the WPT system without MM slab. The measurement results of the fabrication structures in the WPT systems meet well with the tendency of simulations. The small deviation between the experimental and simulation results may be due to the actual radiation loss, fabrication accuracy, MMs' own loss, and measurement errors. It is worth noting that the efficiency improves about 41.7% from 10.6% to 52.3% both in the simulation and measurement at transfer distance of 30 cm (about normalized distances 2.5), when the presented MM slab is used.

Obviously, the PTE is maximized for improvement at distance of 30 cm. Due to enough available space between Tx and Rx, the effect of position of the MM on the WPT is also examined. The results indicate that a high-efficiency WPT system via magnetic resonance is implemented by using the CLSRs structure in the middle as the magnetic flux guide. We may consider placing the MM near the Tx or Rx coil. While, in this case, the efficiency is also partly enhanced, but the MM is strongly coupled to the Tx or Rx resonators, resulting in frequency splitting phenomena [41]. The frequency splitting suppresses energy transmission around the original resonant frequency, leading to efficiency reduction. Therefore, we can place the MM in the middle, where the effect of MM to Tx or Rx resonators is at its maximum.

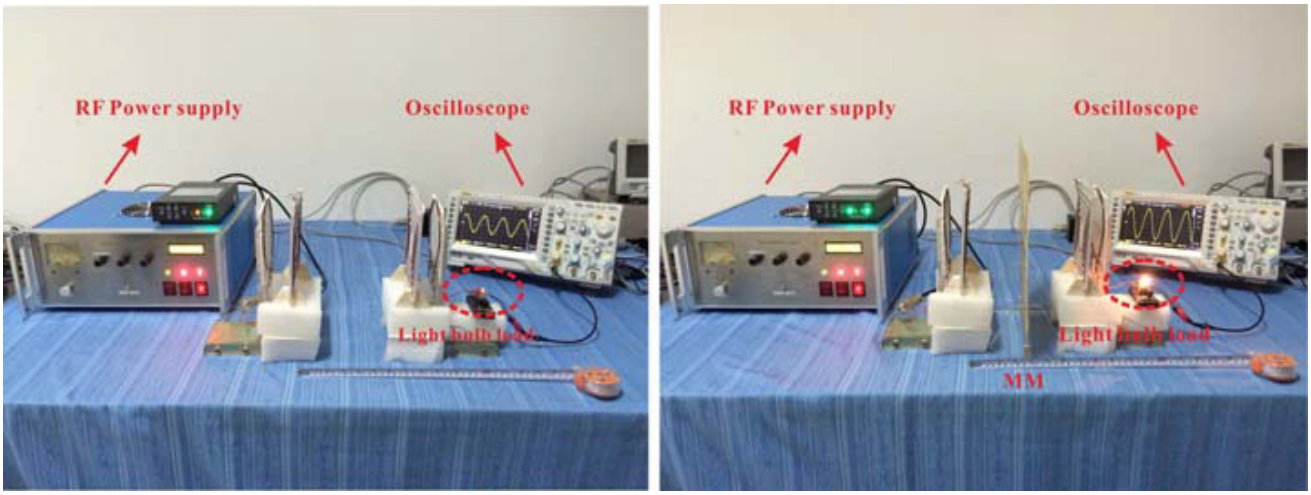


(a) (b)

**Figure 13.** WPT experiment to a 2.8 W light bulb load. (a) Traditional system without MM, (b) system with MM.

Finally, a more practical WPT system with a low power light bulb load was investigated to directly verify the proposed transfer power enhancement. The rated voltage and power of light bulb are 4 V and 2.8 W. The light bulb was connected to the load loop as shown in Figure 13. The transmission distance maintained 30 cm, and the distances between loop antennas and spiral resonators were adjusted for optimal matching. The brightness of light bulb can reflect the amount of power transferred. Two cases of the WPT system were demonstrated with and without MM. The power was provided by the radio frequency (RF) power supply, and the input power was set to 5 W in both cases. The corresponding pictures in Figure 13 were taken in the experiment at same settings. Figure 13(a) shows the original system without MM, where the light bulb barely glows. It is obvious that the bulbs become much brighter in the system implemented MM, as shown in Figure 13(b). These experimental results intuitively verify that PTEs of WPT system are indeed improved significantly by the MM.

## 4. SUMMARY AND DISCUSSIONS

In this work, a metamaterial-based high-efficiency WPT system is designed, simulated and measured in the analysis at 13.56 MHz. The size and performance of the proposed WPT system are compared to some metamaterial-based systems reported previously in Table 2. In fact, it is rather difficult to compare the PTE of various WPT devices with different solutions, coil sizes, transfer distances, transmitted power and frequencies. Generally, the high efficiency enhancement of WPT can be obtained using bulky MMs such as three dimensional MM slabs [15, 18]. Most reported MMs in the literatures [18, 20, 22, 23] may be too thick and large in size for applications in some occasions. In our design, the proposed WPT system has the advantages of miniaturization and ultra-thin structure compared with most early publications. In addition, a relatively high maximum efficiency improvement of 41.7% is obtained by the compact structure. Therefore, we show that the contradiction of limited transfer distance and efficiency can be mitigated using magnetic MM. Therefore, this study deals with an interesting and challenging topic since magnetic MMs have many present and prospect applications in WPT systems. The high efficiency and ultra-thin structure can be useful for applications in future designs with the aim of improving the low power WPT system performance.

**Table 2.** Comparison of metamaterial-based WPT systems.

| Reference ID | MM unit cell size (mm) | Thickness (mm) | PTE enhancement | Working freq. (MHz) |
|---|---|---|---|---|
| [18] | 480 | 120 | 21.05% | 23.20 |
| [20] | 65 | 3 | 30% | 27 |
| [22] | 69 | 19 | 6.93% | 23.7 |
| [23] | 150 | 60 | 34.4% | 6.5 |
| This paper | 140 | 2 | 41.7% | 13.56 |

## 5. CONCLUSION

In conclusion, to achieve a high efficiency WPT system, we investigated an ultra-thin planar magnetic MM working at 13.56 MHz to enhance the PTE and extend effective transfer distance. Theoretical analysis, simulations and experiments all show that the proposed MM has great potential for enhancing the efficiency and mitigating the effects of low efficiency in under coupled region. The simulation results indicate that the contribution of high PTE is due to the property of negative effective permeability which can make the WPT system work in the mechanism of magnetic resonance. The measured efficiencies of the system at different transmission distances are investigated. The experimental results demonstrated that a maximum efficiency improvement of 41.7% can be obtained at transfer distance of 30 cm, by integrating a $2 \times 2$ unit cells MM slab in WPT system. A more practical metamaterial-based wireless power supply device was also presented to intuitively verify the proposed transfer power enhancement. Therefore, a metamaterial-based high-efficiency WPT system is obtained. In addition, large area, homogeneous magnetic field is obtained by the proposed MM. Arbitrary near-field profile and tunable directive near-field pattern by RF magnetic MM are needed to be further investigated in future researches. We believe that the proposed MM, which has the advantages of high efficiency, ultra-thin structure and fabrication simplicity, can find low power portable electronic devices applications in future WPT technology.

## ACKNOWLEDGMENT

This work was supported by the Scientific Projects of State Grid Corporation of China, the Special Funds of State Key Laboratory of Advanced Electromagnetic Engineering and Technology (No. 2015ZZ004), Graduates' Innovation Fund (No. 0118650025), Huazhong University of Science and Technology and the

Youth Science and Technology Backbone Cultivation Plan Project of the Wuhan University of Science and Technology (Grant No. 2016xz010).

## REFERENCES


1. Anderson, L. I., "Nikola Tesla on his work with alternating currents and their application to wireless telegraphy, telephony and transmission of power," *Telephony and Transmission of Power Twenty First Century Books*, 88–147, 2002.
2. Garnica, J., R. A. Chinga, and J. Lin, "Wireless power transmission: From far field to near field," *Proc. IEEE*, Vol. 101, No. 6, 1321–1331, 2013.
3. McSpadden, J. O. and J. C. Mankins, "Space solar power programs and microwave wireless power transmission technology," *IEEE Micro. Mag.*, Vol. 3, No. 4, 46–57, 2002.
4. Kurs, A, A. Karalis, R. Moffatt, J. D. Joannopoulos, P. Fisher, and M. Soljacic, "Wireless power transfer via strongly coupled magnetic resonances," *Science*, Vol. 317, 83–86, 2007.
5. Sample, A. P., D. A. Meyer, and J. R. Smith, "Analysis, experimental results, and range adaptation of magnetically coupled resonators for wireless power transfer," *IEEE Trans. Ind. Electron.*, Vol. 58, No. 2, 544–554, 2011.
6. Chen, L., S. Liu, Y. C. Zhou, and T. J. Cui, "An optimizable circuit structure for high-efficiency wireless power transfer," *IEEE Trans. Ind. Electron.*, Vol. 60, No. 1, 339–349, 2013.
7. Lee, C. K., W. Zhong, and S. Hui, "Effects of magnetic coupling of nonadjacent resonators on wireless power domino-resonator systems," *IEEE Trans. Power Electron.*, Vol. 27, No. 4, 1905–1916, 2012.
8. Ahn, D. and S. Hong, "A study on magnetic field repeater in wireless power transfer," *IEEE Trans. Ind. Electron.*, Vol. 60, No. 1, 360–371, 2013.
9. Che, B. J., G. H. Yang, F. Y. Meng, K. Zhang, J. H. Fu, Q. Wu, and L. Sun, "Omnidirectional non-radiative wireless power transfer with rotating magnetic field and efficiency improvement by metamaterial," *Appl. Phys. A — Mater. Sci. & Processing*, Vol. 116, No. 4, 1579–1586, 2014.
10. Rodríguez, E. S. G., A. K. RamRakhyani, D. Schurig, and G. Lazzi, "Compact low-frequency metamaterial design for wireless power transfer efficiency enhancement," *IEEE Trans. Microw. Theory Techn.*, Vol. 64, No. 5, 1644–1654, 2016.
11. Pham, T. S., A. K. Ranaweera, V. D. Lam, and J. W. Lee, "Experiments on localized wireless power transmission using a magneto-inductive wave two-dimensional metamaterial cavity," *Appl. Phys. Exp.*, Vol. 9, 044101, 2016.
12. Zhang, Y. Y., C. Yao, H. J. Tang, and Y. C. Li, "Spatially mapped metamaterials make a new magnetic concentrator for the two-coil system," *Progress In Electromagnetics Research*, Vol. 150, 49–57, 2015.
13. Cho, Y., J. J. Kim, D. H. Kim, S. Lee, H. Kim, C. Song, S. Kong, H. Kim, C. Seo, S. Ahn, and J. Kim, "Thin PCB-type metamaterials for improved efficiency and reduced EMF leakage in wireless power transfer systems," *IEEE Trans. Microw. Theory Techn.*, Vol. 64, No. 2, 353–364, 2016.
14. Chen, J. F., Z. Y. Hu, S. M. Wang, M. H. Liu, Y. Z. Cheng, Z. X. Ding, B. Wei, and S. C. Wang, "Application of ultra-thin assembled planar metamaterial for wireless power transfer system," *Progress In Electromagnetics Research C*, Vol. 65, 153–162, 2016.
15. Chabalko, M. J., J. Besnoff, and D. S. Ricketts, "Magnetic field enhancement in wireless power with metamaterials and magnetic resonant couplers," *IEEE Antenna Wireless Propag. Lett.*, Vol. 15, 452–455, 2016.
16. Pendry, J. B., "Negative refraction makes a perfect lens," *Phys. Rev. Lett.*, Vol. 85, 3966, 2000.
17. Urzhumov, Y. and D. R. Smith, "Metamaterial-enhanced coupling between magnetic dipoles for efficient wireless power transfer," *Phys. Rev. B*, Vol. 83, No. 20, 205114, 2011.

18. Choi, J. and C. H. Seo, "High-efficiency wireless energy transmission using magnetic resonance based on negative refractive index metamaterial," *Progress In Electromagnetics Research*, Vol. 106, 33–47, 2010.
19. Huang, D., Y. Urzhumov, D. R. Smith, K. H. Teo, and J. Zhang, "Magnetic superlens-enhanced inductive coupling for wireless power transfer," *J. Appl. Phys.*, Vol. 111, No. 6, 064902, 2012.
20. Wang, B., K. H. Teo, T. Nishino, W. Yerazunis, J. Barnwell, and J. Zhang, "Experiments on wireless power transfer with metamaterials," *Appl. Phys. Lett.*, Vol. 98, No. 25, 254101, 2011.
21. Wang, B., W. Yerazunis, and K. H. Teo, "Wireless power transfer: Metamaterials and array of coupled resonators," *Proc. IEEE*, Vol. 101, No. 6, 1359–1368, 2013.
22. Lipworth, G., J. Ensworth, K. Seetharam, D. Huang, J. S. Lee, P. Schmalenberg, T. Nomura, M. S. Reynolds, D. R. Smith, and Y. Urzhumov, "Magnetic metamaterial superlens for increased range wireless power transfer," *Sci. Rep.*, Vol. 4, 3642, 2014.
23. Ranaweera, A. L. A. K., T. P. Doung, and J. W. Lee, "Experimental investigation of compact metamaterial for high efficiency midrange wireless power transfer applications," *J. Appl. Phys.*, Vol. 116, No. 4, 043914, 2014.
24. Ranaweera, A. L. A. K., C. A. Moscoso, and J. W. Lee, "Anisotropic metamaterial for efficiency enhancement of mid-range wireless power transfer under coil misalignment," *J. Phys. D: Appl. Phys.*, Vol. 48, No. 45, 455104, 2015.
25. Chen, W. C., C. M. Bingham, K. M. Mak, N. W. Caira, and W. J. Padilla, "Extremely subwavelength planar magnetic metamaterials," *Phys. Rev. B*, Vol. 85, No. 20, 201104, 2012.
26. Bilotti, F., A. Toscano, and L. Vegni, "Design of spiral and multiple split-ring resonators for the realization of miniaturized metamaterial samples," *IEEE Trans. Antennas Propag.*, Vol. 55, No. 8, 2258–2267, 2007.
27. Baena, J. D., R. Marques, F. Medina, and J. Martel, "Artificial magnetic metamaterial design by using spiral resonators," *Phys. Rev. B*, Vol. 69, No. 1, 014402, 2004.
28. Huang, Y., H. J. Tang, E. C. Chen, and C. Yao, "Effect on wireless power transmission with different layout of left-handed materials," *AIP Adv.*, Vol. 3, No. 7, 072134, 2013.
29. Smith, D. R., D. C. Vier, Th. Koschny, and C. M. Soukoulis, "Electromagnetic parameter retrieval from inhomogeneous metamaterials," *Phys. Rev. E*, Vol. 71, No. 3, 036617, 2005.
30. Smith, D. R., S. Schultz, P. Markoš, and C. M. Soukoulis, "Determination of effective permittivity and permeability of metamaterials from reflection and transmission coefficients," *Phys. Rev. B*, Vol. 65, No. 19, 195104, 2002.
31. Wu, Q., Y. H. Li, N. Gao, F. Yang, Y. Q. Chen, K. Fang, Y. W. Zhang, and H. Chen, "Wireless power transfer based on magnetic metamaterials consisting of assembled ultra-subwavelength meta-atoms," *EPL-Europhys. Lett.*, Vol. 109, No. 6, 68005, 2015.
32. Cheng, Y. Z., J. Jin, W. L. Li, J. F. Chen, B. Wang, and R. Z. Gong, "Indefinite-permeability metamaterial lens with finite size for miniaturized wireless power transfer system," *Int. J. Electron. Commun. (AEÜ)*, Vol. 70, No. 9, 1282–1287, 2016.
33. Fan, Y., L. Li, S. Yu, C. Zhu, and C. H. Liang, "Experimental study of efficient wireless power transfer system integrating with highly sub-wavelength metamaterials," *Progress In Electromagnetics Research*, Vol. 141, 769–784, 2013.
34. Son, H. C., J. W. Kim, D. H. Kim, K. H. Kim, and Y. J. Park, "Self-resonant coil with coaxial-like capacitor for wireless power transfer," *IEEE Microw. Conf. Proc. (APMC)*, 90–93, Asia-Pacific, 2011.
35. Kalantarov, P. L. and L. A. Zeitlin, *Inductances Calculation Handbook*, 1986, translated by T. Chen, et al., China Machine Press, Beijing, 1992 (in Chinese).
36. Lyu, Y. L., F. Y. Meng, G. H. Yang, B. J. Che, Q. Wu, L. Sun, D. Erni, and J. L. W. Li, "A method of using nonidentical resonant coils for frequency splitting elimination in wireless power transfer," *IEEE Trans. Power Electron.*, Vol. 30, No. 11, 6097–6107, 2015.
37. Mongia, R., *RF and Microwave Coupled-Line Circuits*, Artech House, Norwood MA, 2007.
38. Chen, J., *Feedback Networks: Theory and Circuit Application*, World Scientific, Singapore, 2007.

39. Freire, M. J. and R. Marques, "Planar magnetoinductive lens for three-dimensional subwavelength imaging," *Appl. Phys. Lett.*, Vol. 86, 182505, 2005.
40. Duong, T. P. and J. W. Lee, "Experimental results of high-efficiency resonant coupling wireless power transfer using a variable coupling method," *IEEE Microw. Wireless Compon. Lett.*, Vol. 21, No. 8, 442–444, 2011.
41. Niu, W. Q., W. Gu, J. X. Chu, and A. D. Shen, "Coupled-mode analysis of frequency splitting phenomena in CPT systems," *Electron. Lett.*, Vol. 48, No. 12, 723–724, 2012.